Final-state-resolved mutual neutralization of Na$^+$ and D$^-$

Gustav Eklund ⓘ,[1,*] Jon Grumer ⓘ,[2] Paul S. Barklem ⓘ,[2] Stefan Rosén,[1] MingChao Ji ⓘ,[1] Ansgar Simonsson ⓘ,[1]
Richard D. Thomas ⓘ,[1] Henrik Cederquist ⓘ,[1] Henning Zettergren,[1] and Henning T. Schmidt ⓘ[1,†]

[1]*Department of Physics, Stockholm University, Stockholm, 10691, Sweden*
[2]*Theoretical Astrophysics, Department of Physics and Astronomy, Uppsala University, Uppsala, 75237, Sweden*

The present paper reports on a merged-beam experiment on mutual neutralization between Na$^+$ and D$^-$. For this experiment, we have used the DESIREE ion-beams storage-ring facility. The reaction products are detected using a position- and time-sensitive detector, which ideally allows for determination of the population of each individual quantum state in the final atomic systems. Here, the $4s$, $3d$, and $4p$ final states in Na are observed and in all cases the D atom is in its ground state $1s\,^2S$. The respective branching fractions of the states populated in Na are determined by fitting results from a Monte Carlo simulation of the experiment to the measured data. The center-of-mass collision energy is controlled using a set of biased drift tubes, and the branching fractions are measured for energies between 80 meV and 393 meV. The resulting branching fractions are found to agree qualitatively with the only available theoretical calculations for this particular system, which are based on a multichannel Landau-Zener approach using dynamic couplings determined with a linear combination of atomic orbitals model.

I. INTRODUCTION

Atomic and molecular collision processes involving ions, neutrals, or electrons play a fundamental role in a wide range of fields including astrophysics [1–8], plasma physics [9,10], chemical reactions [11,12], and radiation protection [13]. The present paper is focused on the process of mutual neutralization (MN)—a charge-transfer reaction in which a cation, A$^+$, and an anion, B$^-$, collide at meV center-of-mass kinetic energies and neutralize through the transfer of an electron. The resulting neutral products are distributed in various final states depending on the available energy and the possible quasimolecular states and their coupling in the collision. Such a process will from here on be abbreviated A$^+$/B$^-$. In this paper, we investigate the MN reaction between sodium cations and deuterium anions, Na$^+$/D$^-$, through a final-state-resolved merged-beam experiment at the DESIREE cryogenic ion-beams storage-ring facility at Stockholm University, Sweden [14,15].

The measurement of Na abundances in stars is an important problem in astrophysics. Na is produced through carbon burning (^{12}C(^{12}C, p)^{23}Na) in short-lived massive stars, leading to a relatively large astrophysical abundance. This large abundance results in a number of observable Na signatures in stellar spectra, including the famous D $3s − 3p$ resonance lines that are among the strongest features in the solar spectrum. Very different abundance ratios of Na to other astrophysically important elements (e.g., oxygen) in globular clusters compared to the bulk of our galaxy indicates that the chemical evolution scenario in dense stellar clusters are of a different nature than in galactic disks. Thus, accurate Na abundances from interpretation of stellar spectra are also of large importance (see, e.g., Gratton *et al.* [16]).

The Na *D* lines in the sun were, in fact, the first case for which nonlocal thermodynamical equilibrium (non-LTE) modeling including both radiative and collisional processes had to be used to explain the observations. Plaskett [17] considered electron and hydrogen collisions to explain Na *D*-line intensities [i.e., Na(3s) + e$^-$ → Na(3p) + e$^-$, and Na(3s) + H → Na(3p) + H], but based on the Massey criterion [18] they concluded that collisions with atomic hydrogen were unlikely to be important. The importance of MN between Na$^+$ and H$^-$ and the inverse process of ion-pair production was recognized very early in the atomic physics community [19–22]. However, it was not until much later that the possible importance of these processes in stellar atmospheres, and thus in interpreting accurate stellar Na abundances, was highlighted by Barklem *et al.* [23]. These ideas were later applied to a large grid of stellar-spectrum calculations by Lind *et al.* [24]. These astrophysical applications use MN rate coefficients from the FQ-scattering model by Belyaev *et al.* [25] based on the structure calculations by Dickinson *et al.* [22]. This methodology is analogous to the theoretical approach developed for MN between Li$^+$ and H$^-$ by Belyaev and Barklem [26]. Apart from being an important process in stellar atmospheres, MN is also believed to influence the

*gustav.eklund@fysik.su.se
†schmidt@fysik.su.se

ionization in the early universe, as well as the chemistry in the interstellar medium and in planetary atmospheres [27,28].

Experimental investigations of MN processes are scarce. Earlier studies focused primarily on determining the total cross section for MN at different initial center-of-mass collision energies [29]. These experiments were limited by (1) relatively high center-of-mass collision energies, thus excluding the low-energy range (<1 eV) of main interest for many astrophysical applications, and (2) the inability to distinguish between different final states and reaction channels. Recent developments have partially overcome these limitations by combining merged-beam methods with imaging detector techniques, opening up for more detailed studies of MN and other charge- and mass-transfer reactions. Such imaging techniques allow for detection of two or more reaction products in coincidence and measurements of the kinetic-energy release, E_K, of the reaction which provides information on the initial and final quantum states. These types of detection schemes have been used in single-pass experiments on the MN of O^+/O^- [30] and Li^+/D^- [31], and recently also with two stored ion beams to measure MN for the Li^+/D^- system at DESIREE [32].

In the present work at DESIREE following Li^+/D^-, we turn to the slightly more complex, yet similar in terms of the types of electron transfer processes, MN between Na^+ and D^-,

$$Na^+(2p^6) + D^-(1s^2) \rightarrow Na(2p^6 nl) + D(1s) + E_K(nl),$$
$$(1)$$
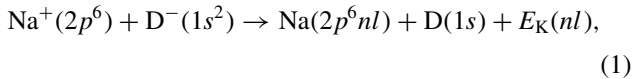
where the incoming ions are in their ground states at the time of collision, and the kinetic-energy release $E_K(nl)$ is determined by the $nl\ ^{2S+1}L$ state of the outgoing Na atoms. In DESIREE, there is a practical upper limit to the ratio of the kinetic energies of the two ion beams of about 20 [14]. To reach low center-of-mass energies, this condition translates to a similar ratio of the masses of the two ion species. For this reason, we choose to use D^- instead of H^-, where the latter is the anion of main interest for astrophysical applications. At zero center-of-mass collision energy, the energy available through the exothermic MN reaction in Na^+/D^- is given by the difference between the electron affinity of D (0.75459(87) eV [33]) and the ionization energy of Na (5.1390769(3) eV [34,35]). This difference is 4.38 eV, which is sufficient to form the Na atom (but not the D atom) in an excited state.

II. EXPERIMENT

The DESIREE merged-beam setup has been described in detail previously [14,15,32]. A schematic of the setup with the two ion-beams storage rings and their common straight section for merged-beam experiments is shown in Fig. 1. For the present experiment, Na^+ is produced from an electron cyclotron resonance ion source using a powder of NaBr heated in an oven. The Na^+ beam is extracted from the source and accelerated to 47.992 keV. The D^- ions are produced from a TiD cathode using a Source of Negative Ions by Cesium Sputtering and accelerated to 4.975 keV. Note that the beam energies given here are based on measurements of the acceleration voltage on the ion source platforms. The ion beams are
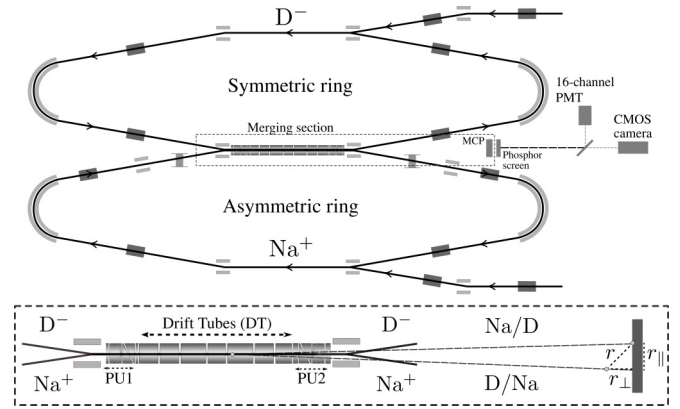
FIG. 1. A schematic of the DESIREE storage rings. Na^+ ions are stored in the asymmetric ring and D^- ions are stored in the symmetric ring. The two beams are overlapped in the merging section where the mutual neutralization reaction occurs. The center-of-mass collision energy $E_{c.m.}$ is controlled using a set of biased electrodes. The resulting neutral products are detected using an imaging detector system consisting of a microchannel plate (MCP) assembly, a phosphor screen, a 16-channel photomultiplier tube (PMT), and a CMOS camera (see text).

injected into the asymmetric and symmetric rings as indicated in Fig. 1. The storage lifetimes and the overlap between the two ion beams are optimized using a set of pickup electrodes (measuring beam positions) and the signals from two Faraday cups detecting the ions when they are ejected from the rings. For the MN measurements, the ion beams are stored for five seconds before being ejected from the rings. The MN products are measured continuously during storage using an imaging detector, consisting of a triple-stack microchannel plate with a phosphor screen anode [36]. The light from the phosphor screen is guided through the windows of the DESIREE vacuum chambers [14]. An optical beam splitter is used to direct the light onto a Complementary Metal Oxide Semiconductor (CMOS) camera to detect the positions of the products on the detector and onto a 16-channel photomultiplier tube (PMT) for determination of the time of flight difference, Δt, of the products.

For two particles A and B, the center-of-mass collision energy, $E_{c.m.}$, is given by

$$E_{c.m.} = \mu \left[\frac{E_A}{m_A} + \frac{E_B}{m_B} - 2\sqrt{\frac{E_A E_B}{m_A m_B}} \cos \alpha \right], \quad (2)$$

where μ is the reduced mass, E_A and E_B are the kinetic energies of the particles, m_A and m_B are their respective masses, and α is the angle between the particle trajectories. With the ion beam energies of 47.992 keV for Na^+ and 4.975 keV for D^- and assuming the trajectories of the ions are parallel, Eq. (2) gives $E_{c.m.} \approx 31$ eV. The center-of-mass collision energy can be locally controlled by a set of drift tubes in the merging section of the two rings. For the current experiment, the three middle electrodes are biased, such that the ions have a low and controlled value of $E_{c.m.}$ in an interaction region with a length of 24.4 cm. According to Eq. (2), $E_{c.m.}$ has a minimum when the velocities of the particles are equal. For the present beam energies, the velocities are expected to match

when the drift tube bias voltage, U_{DT}, has a value of -708 V. However, the expected U_{DT} where the velocities match may have a small offset due to uncertainties in the measurements of U_{DT} as well as the kinetic energies of the two ion beams. Experimentally, the minimum is found by measuring the rate of the MN signal as a function of U_{DT}, relying on the expected $1/E_{c.m.}$ energy dependence of the cross section at low $E_{c.m.}$ [37]. These measurements may also be used to determine $E_{c.m.}$ as a function of U_{DT} as discussed in Sec. IV. Additional measurements are then performed at high statistics to determine the branching fractions (BFs) of the final states for a set of collision energies. A more detailed description of the experimental technique can be found in Ref. [32].

III. THEORETICAL CONSIDERATIONS

Theoretical predictions of Na^+/D^- at low energies are so far limited to the set of asymptotic model, multichannel Landau-Zener calculations by Barklem *et al.* [38]. These calculations include two methods for determining the couplings at the avoided crossings of quasimolecular states: one which adopts semiempirical results from Ref. [39], while the other method is based on a two-electron linear combination of atomic orbitals (LCAO) approach [40,41]. No full-quantum (FQ) calculations, i.e., quantum scattering modeling based on quantum chemistry molecular structure calculations, on collisions on Na^+ with D^- have been carried out; only with H^- by Belyaev *et al.* [25]. These are based on the potentials and couplings from the molecular structure calculations by Dickinson *et al.* [22].

The effect of Coulomb focusing is generally expected to significantly increase the total cross section for MN with H^- as compared to MN with D^-. This increase is due to a shorter distance of closest approach between the reactants in the case of the lighter anion. The impact on the BFs is expected to be smaller than the impact on the total cross section, but can have significant contributions of up to 5% in the case of $Na^+ + H^-$ or D^- as shown by the analysis of Barklem *et al.* [38]. Although FQ results are, in general, expected to be more reliable, it is also clear from Ref. [38] that the difference between the predictions of the FQ and asymptotic models, LCAO in particular, is smaller than the isotopic effects in the energy regime of interest here. We shall therefore mainly use the LCAO results on D^- collisions for comparisons. A more elaborate study of the performance of various available theoretical models for both isotopes is given in Barklem *et al.* [38], which also discusses the impact of H^- versus D^- on the MN collision strength in astrophysical applications.

Term-averaged excitation energies for the final Na atomic states, E_{av} with corresponding kinetic energy releases, E_K, are given in Table I together with BFs for Na^+/D^- over a range of relevant collision energies as predicted by the asymptotic LCAO model [38] mentioned above. Judging from these and the earlier FQ results by Belyaev *et al.* [25], the theory-based expectation is that the distribution over final states should stay roughly constant over the energy range under investigation and be dominated by the channels around $E_K = 1$ eV with the $4s$ final state contributing with $\sim 82\%$, followed by $3d$ at $\sim 14\%$, $4p$ at $\sim 3.5\%$, and $3p$ at $\sim 0.2-0.5\%$. The remaining channels are expected to have BFs $<0.1\%$.

TABLE I. Relevant energy structure of $Na(2p^6\,{}^1S_0\,nl)$ including the first ionization limit, $Na^+(2p^6\,{}^1S_0)$, where E_{av} are term-averaged excitation or ionization energies as listed by the NIST ASD [42]. $E_K(nl)$ is the corresponding kinetic energy release of the MN reaction in Eq. (1). The four last columns list predicted MN branching fractions for the $Na(nl)$ final states for a selection of nonzero center-of-mass collision energies, $E_{c.m.}$, spanning the low-energy range of interest in this paper up to c.a. 1 eV (11605 K), derived from the Na^+/D^- LCAO calculations of Barklem *et al.* [38]. Note that these BFs do not necessarily sum up to unity due to round-off errors.

	nl	E_{av} [eV]	E_K [eV]	BF[a] [%]/$E_{c.m.}$ [meV]			
				50	250	500	1000
Na	$3s$	0	4.38	0.0	0.0	0.0	0.0
	$3p$	2.10	2.28	0.4	0.4	0.6	0.8
	$4s$	3.19	1.19	81.1	81.5	81.4	81.4
	$3d$	3.62	0.77	14.9	14.5	14.5	14.3
	$4p$	3.75	0.63	3.6	3.6	3.6	3.6
	$5s$	4.12	0.27	0.0	0.0	0.0	0.0
Na^+	–	5.14					

[a]Theoretical values from Barklem *et al.* [38].

IV. RESULTS AND ANALYSIS

A. Assignment of channels and center-of-mass collision energy

The detected products from the MN reaction are recorded on an event-by-event basis. For each event, the positions of the atoms in the detector plane and the triggered channels on the PMT are recorded. In the analysis, we consider events where the CMOS camera detects two particles, and where more than a single channel on the PMT has been triggered. The time of flight difference, Δt, is determined from the time between the two PMT signals. Due to the finite resolution of the detection system, events with $\Delta t < 5$ ns are rejected [32].

To connect the total kinetic energy of the system after the MN reaction has occurred to a quantity that can be measured in the experiment, we define the distance between the products, r. The total kinetic energy after the collision may then be expressed as

$$E_{c.m.} + E_K(nl) = \frac{\mu}{2}\left(\frac{rV}{L}\right)^2, \qquad (3)$$

where μ is the reduced mass, V is the velocity of the center of mass, and L is the distance between the point where the interaction took place and the center of mass of the neutrals. Note that all quantities in Eq. (3) are constant except r and L, implying that r/L is constant, thus the separation increases as the neutrals travel along their trajectories.

In the experiment, the positions of the products on the detector and the corresponding time-of-flight difference are recorded. The distance L cannot be determined for individual events, since the MN process occurs along the entire interaction region, the finite length of which results in a distribution of r values. Now, let $\overline{L}$ be the average distance between the point of interaction and the detector, corresponding to the distance between the center of the interaction region and the detector, $\overline{L} = 1.683 \pm 0.010$ m. The uncertainty in $\overline{L}$ is due to the possible change in overlap due to misalignment of the two
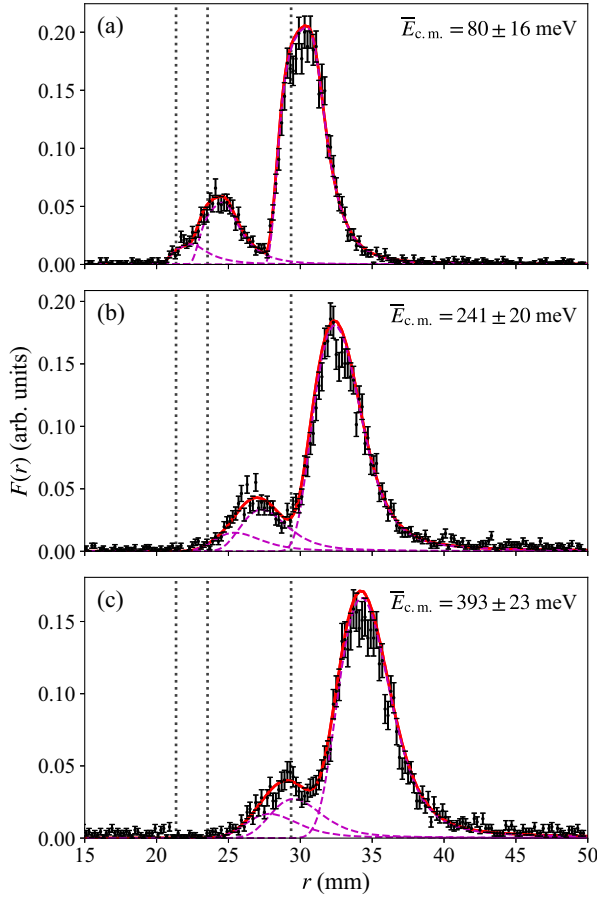
FIG. 2. Measured r distributions at (a) $E_{c.m.} = 80 \pm 16$ meV, (b) $E_{c.m.} = 241 \pm 20$ meV, and (c) $E_{c.m.} = 393 \pm 23$ meV. The small peak at low r is assigned to the $3d$ and $4p$ final states in Na, and the large peak at high r is assigned to the $4s$ state. The vertical dotted lines show the expected average value of r for the assigned states for $\overline{E}_{c.m.} = 0$ eV. The solid red lines represent model distributions described in Sec. IV B fitted to the data to extract BFs, where the purple dashed lines are the individual contributions from the individual states.

ion beams. Let $\overline{r}(nl)$ be the average value of the r distribution for final state nl, and let $\overline{E}_{c.m.}$ be the average center-of-mass collision energy. By replacing the quantities in Eq. (3) with their corresponding averages and solving for $\overline{r}(nl)$, we get

$$\overline{r}(nl) = \sqrt{\frac{2[\overline{E}_{c.m.} + E_K(nl)]}{\mu} \frac{\overline{L}}{V}}, \tag{4}$$

from which the experimental values of $\overline{r}(nl)$ can be predicted. The definition of $\overline{L}$ implies that r should be measured at the point in time when the center of mass of the reaction products arrive at the detector, which is not possible in practice. Experimentally, and referring to Fig. 1, r is approximated from the product positions and Δt in the following way. The distance between the products in the detector plane, $r_\parallel$, is determined. From Δt, the perpendicular separation, $r_\perp$, is calculated as $r_\perp = V \Delta t$. From these quantities, r is given by $r = \sqrt{r_\perp^2 + r_\parallel^2}$.
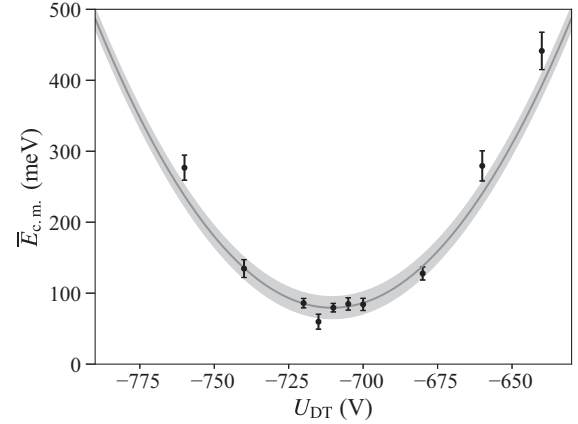
FIG. 3. Measured average center-of-mass collision energy, $\overline{E}_{c.m.}$, as a function of drift tube bias voltage, U_{DT}. The line is a fit to Eq. (2). The shaded area indicates the systematic uncertainty resulting from the approximation of the distance between the point of interaction and the detector $\overline{L}$.

The measured r distributions are shown in Fig. 2 along with simulations (full red lines and dashed lines) to be discussed in Sec. IV B. In Fig. 2(a), the measurement is performed with $U_{DT} = -710$ V, resulting in the lowest value of $\overline{E}_{c.m.}$ achieved in the experiment. Figures 2(b) and 2(c) are measured with $U_{DT} = -660$ V and $U_{DT} = -640$ V, respectively. The spectra in Fig. 2 show two distinct features between $r \approx 20$ mm and $r \approx 45$ mm. Using Eq. (4) to calculate the expected r for the $4s$, $3d$, and $4p$ final states of Na we find 29.3, 23.5, and 21.3 mm, respectively, where we tentatively assume that $\overline{E}_{c.m.} = 0$ eV and that V is given from the energies of the two ion beams. These distances are indicated by the vertical dotted lines in Fig. 2. We thus assign the larger feature to $4s$ and the smaller feature to a combination of $3d$ and $4p$. No structure is observed that would correspond to the formation of $3p$ with a predicted r of 40.6 mm, confirming the theoretical prediction that this channel is weak. The shift in r with respect to the expected values seen in Fig. 2(a) and the increase in r observed in Figs. 2(b) and 2(c) are due to the increased value of $\overline{E}_{c.m.}$ which is evident from Eq. (4).

To determine $\overline{E}_{c.m.}$ from the measured r spectra, the dominant $4s$ final state peak is fitted using a Gaussian function and its center position is used as an estimate of $\overline{r}(4s)$. Equation (4) is then used to estimate $\overline{E}_{c.m.}$. The estimated values of $\overline{E}_{c.m.}$ as a function of U_{DT} are shown in Fig. 3. Equation (2) is fitted to the data in Fig. 3 to obtain an average angle between the beams $\overline{\alpha} = 4.5 \pm 0.5$ mrad. Note that $\overline{\alpha}$ does not reflect an actual angle between the two beams, since Eq. (2) is valid for a single collision between two particles, rather $\overline{\alpha}$ is an effective average angle with contributions from an angle between the beams and the divergences of either beam. Furthermore, Eq. (4) depends on $\overline{L}$, and the uncertainty in $\overline{L}$ thus affects the measured values of $\overline{E}_{c.m.}$. The uncertainty in $\overline{L}$ is accounted for by performing the above analysis as a function of $\overline{L}$ within the interval given by its uncertainty. This systematic uncertainty is indicated in Fig. 3 by the shaded area. For the measurements in Fig. 2, $E_{c.m.}$ is calculated from Eq. (2) using the fitted parameters, and the statistical and sys-

tematic uncertainties are added in quadrature, resulting in the assignment of $\overline{E}_{c.m.} = 80 \pm 16$ meV, $\overline{E}_{c.m.} = 241 \pm 20$ meV, and $\overline{E}_{c.m.} = 393 \pm 23$ meV to the distributions in Figs. 2(a)–2(c), respectively.

B. Branching fractions

The relative number of events measured in each peak in Fig. 2 is proportional to the BF, BF(nl), of the final state, nl, of atomic Na. As discussed in the previous section, the large peak at high r is assigned to the 4s state and the smaller peak is assigned to the 3d and 4p states. If the channels were completely separated in the r spectrum, one could determine BF(nl) by simply counting the number of events in each channel. For the present experiment, it is not possible to separate all three channels completely, and to extract BF(nl), the spectra need to be modeled. Let $f_{nl}(r, E_{c.m.})$ represent the r distribution for final state nl at a given $E_{c.m.}$, normalized such that

$$\int_{-\infty}^{\infty} f_{nl}(r, E_{c.m.}) \, dr = 1. \tag{5}$$

The distribution in r for all final states, $F(r, E_{c.m.})$, is then constructed as a linear combination of the distributions $f_{nl}(r, E_{c.m.})$ weighted by the corresponding BF(nl):

$$F(r, E_{c.m.}) = \sum_{nl} BF(nl) f_{nl}(r, E_{c.m.}). \tag{6}$$

The distributions $f_{nl}(r, E_{c.m.})$ are generated from Newtonian Monte Carlo simulations of the experiments as described in Ref. [32]. The simulation is performed by generating events at random positions within the region where the two beams overlap. The initial velocities are determined from the ion-beam energies and are modified according to the potential in the drift tubes. The drift tube potential is a function of the longitudinal position in the drift tubes and it is modeled using the ion optics simulation software SIMION [43]. The longitudinal energy spreads of the ion beams are modeled by Gaussian distributions centered at the beam energies with standard deviations $\sigma_E = 0.15 \pm 0.05\%$ of the beam energies. In addition, the initial transverse velocities of the ions are modeled using a Maxwell-Boltzmann distribution with a temperature of 1100 K for both beams. The expected $1/\sqrt{E_{c.m.}}$ dependence on the MN rate coefficient is accounted for by calculating $E_{c.m.}$ for each event, and accepting the event with a probability proportional to $1/\sqrt{E_{c.m.}}$. The final velocity vectors of the products are calculated by adding the additional momentum resulting from the kinetic energy release of the reaction. Finally, the time-of-flight difference and positions of the products on the detector are calculated, from which the simulated r distribution is generated.

Equation (6) is fitted to the recorded spectra using the method of linear least squares with BF(4s) and BF(3d) as free parameters, which is sufficient since $\sum_{nl} BF(nl) = 1$. The resulting total distributions $F(r, E_{c.m.})$ are shown in Fig. 2 (red lines) along with the contributions from each of the fitted channels $f_{nl}(r, E_{c.m.})$ (dashed purple lines). The estimated uncertainties for BF(nl) from the fit alone are likely to underestimate the total error of the measured BF(nl) since they do not include any error estimations on the simulated $f_{nl}(r, E_{c.m.})$ themselves. To estimate these contributions to the total error,

TABLE II. Summary of the present experimental branching fractions extracted from the data in Fig. 2 as functions of the drift tube bias voltage, U_{DT}, and the center-of-mass collision energy, $E_{c.m.}$. See the text for details on the extraction procedure.

U_{DT} [V]	$E_{c.m.}$ [meV]	BF(nl) [%]		
		4s	3d	4p
−710	80 ± 16	76.8 ± 0.7	17.7 ± 0.9	5.6 ± 0.8
−660	241 ± 20	78.7 ± 1.5	14.6 ± 1.9	6.7 ± 3.1
−640	393 ± 23	78.5 ± 3.0	13.1 ± 1.4	8.3 ± 2.8

the above analysis is repeated using different $f_{nl}(r, E_{c.m.})$, where the simulation parameters are perturbed within their estimated uncertainties. The parameter space for the simulation is rather large and, to simplify the problem, the perturbation analysis is constrained to two parameters, the drift tube voltage U_{DT} and the energy spread of the ion beams σ_E. The justification for the choice of these parameters is that they are the most sensitive parameters in controlling the position (U_{DT}) and width (σ_E) of $f_{nl}(r, E_{c.m.})$. The perturbations used are ±3 V for U_{DT} and ±0.05% for σ_E. The perturbation results in a two-dimensional grid with nine separate fits for each spectrum in Fig. 2, and the resulting spread in fitted BFs are taken as the perturbation error. For the total uncertainty, the statistical uncertainty from the fit is added in quadrature with the error obtained from the perturbation analysis. The final results for the BFs are summarized in Table II and shown in Fig. 4 as a function of $\overline{E}_{c.m.}$ along with the theoretical predictions (dashed lines) from Table I. The measured BFs do not show any significant dependence on $E_{c.m.}$ over the measured energy
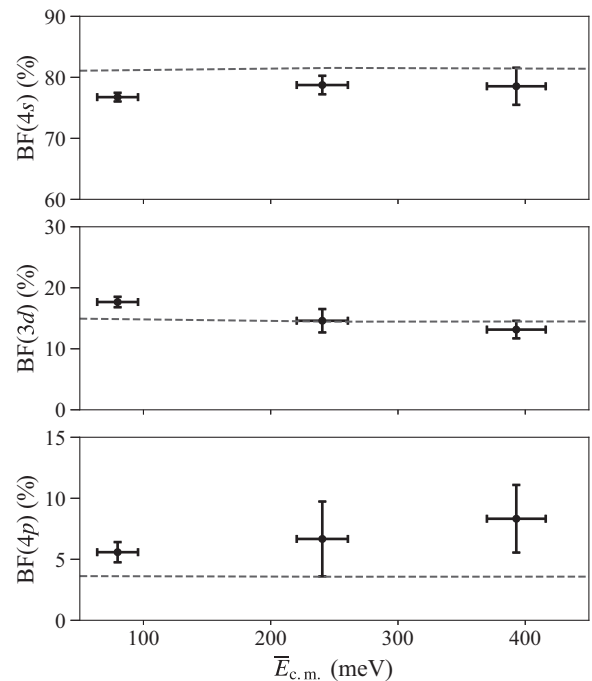
FIG. 4. Measured branching fractions BF(nl) as functions of the center-of-mass collision energy $E_{c.m.}$. The dashed lines are the theoretical BF(nl) from Barklem *et al.* [38].

range, which is consistent with the theoretical prediction [38]. The 4*s* channel dominates, as predicted by theory, however, it appears that the theory slightly overestimates the BF for this state.

V. CONCLUSIONS

Following the pilot study of Li$^+$/D$^-$ at the DESIREE double electrostatic and cryogenic storage-ring facility at Stockholm University [32], we here report on a merged-beam experiment of the MN between Na$^+$ and D$^-$. Low-energy collision measurements between these reactants were recently made possible due to improved ion-beam optimization routines at DESIREE, allowing ions with large mass ratios to be stored at similar velocities. Since Na$^+$/D$^-$ represents a similar electron transfer process as that of Li$^+$/D$^-$, where both have been investigated earlier using the same theoretical framework, Na$^+$/D$^-$ provides a systematic continuation of MN investigations at energies of relevance for astrophysical modeling of, for example, stellar atmospheres. More details on the impact of the various experimental and theoretical results for both these systems in an astrophysical context, such as the impact on the Na *D* lines, is discussed by Barklem *et al.* [38].

In the present experiment, MN was measured at center-of-mass collision energies between 80 meV and 393 meV (928 K and 4561 K). The 4*s*, 3*d*, and 4*p* final states of Na were observed, which are the dominant states predicted from theory. Despite only partially resolving the 3*d* and 4*p* states, BFs were determined for all observed states using an analysis based on Newtonian Monte Carlo simulations of the collision process. No significant energy dependence was observed in this low-energy range. The BFs qualitatively agree with the FQ calculations for Na$^+$/H$^-$ by Belyaev *et al.* [25] and the LCAO calculations presented in Barklem *et al.* [38]. Given the, at DESIREE, unprecedented high mass ratio, and agreement of the obtained BFs with theoretical models, these results also provide an important stepping stone for further MN experiments at DESIREE.

[1] P. S. Barklem, Accurate abundance analysis of late-type stars: Advances in atomic physics, Astron. Astrophys. Rev. **24**, 9 (2016).

[2] C. M. Lisse, K. Dennerl, J. Englhauser, M. Harden, F. E. Marshall, M. J. Mumma, R. Petre, J. P. Pye, M. J. Ricketts, J. Schmitt, J. Trümper, and R. G. West, Discovery of X-ray and extreme ultraviolet emission from comet C/Hyakutake 1996 B2, Science **274**, 205 (1996).

[3] P. Chaizy, H. Reme, J. Sauvaud, C. d'Uston, R. Lin, D. Larson, D. Mitchell, K. Anderson, C. Carlson, A. Korth *et al.*, Negative ions in the coma of comet Halley, Nature **349**, 393 (1991).

[4] E. Zipf, P. Espy, and C. Boyle, The excitation and collisional deactivation of metastable N(^2P) atoms in auroras, J. Geophys. Res.: Space Phys. **85**, 687 (1980).

[5] M. H. Rees and R. G. Roble, Excitation of O(1D) atoms in aurorae and emission of the [OI]6300-Å line, Can. J. Phys. **64**, 1608 (1986).

[6] D. Koutroumpa, R. Lallement, V. Kharchenko, A. Dalgarno, R. Pepino, V. Izmodenov, and E. Quémerais, Charge-transfer induced EUV and soft x-ray emissions in the heliosphere, Astron. Astrophys. **460**, 289 (2006).

[7] D. Koutroumpa, F. Acero, R. Lallement, J. Ballet, and V. Kharchenko, OVII and OVIII line emission in the diffuse soft x-ray background: Heliospheric and galactic contributions, Astron. Astrophys. **475**, 901 (2007).

[8] E. Moebius, D. Rucinski, D. Hovestadt, and B. Klecker, The helium parameters of the very local interstellar medium as derived from the distribution of He$^+$ pickup ions in the solar wind, Astron. Astrophys. **304**, 505 (1995).

[9] R. C. Isler, An overview of charge-exchange spectroscopy as a plasma diagnostic, Plasma Phys. Controlled Fusion **36**, 171 (1994).

[10] U. Fantz, P. Franzen, and D. Wünderlich, Development of negative hydrogen ion sources for fusion: Experiments and modelling, Chem. Phys. **398**, 7 (2012), Chemical Physics of Low-Temperature Plasmas (in honour of Prof. Mario Capitelli).

[11] S. S. Prasad and W. T. Huntress, Jr., A model for gas phase chemistry in interstellar clouds: I. The basic model, library of chemical reactions, and chemistry among C, N, and O compounds, Astrophys. J., Suppl. Ser. **43**, 1 (1980).

[12] A. Yoshimori, T. Kakitani, Y. Enomoto, and N. Mataga, Shapes of the electron-transfer rate vs energy gap relations in polar solutions, J. Phys. Chem. **93**, 8316 (1989).

[13] D. Goodhead, Initial events in the cellular effects of ionizing radiations: Clustered damage in DNA, Int. J. Radiat. Biol. **65**, 7 (1994).

[14] R. D. Thomas, H. T. Schmidt, G. Andler, M. Björkhage, M. Blom, L. Brännholm, E. Bäckström, H. Danared, S. Das, N. Haag *et al.*, The double electrostatic ion ring experiment: A unique cryogenic electrostatic storage ring for merged ion-beams studies, Rev. Sci. Instrum. **82**, 065112 (2011).

[15] H. T. Schmidt, R. D. Thomas, M. Gatchell, S. Rosén, P. Reinhed, P. Löfgren, L. Brännholm, M. Blom, M. Björkhage, E. Bäckström *et al.*, First storage of ion beams in the double electrostatic ion-ring experiment: Desiree, Rev. Sci. Instrum. **84**, 055115 (2013).

[16] R. Gratton, C. Sneden, and E. Carretta, Abundance variations within globular clusters, Annu. Rev. Astron. Astrophys. **42**, 385 (2004).

[17] H. H. Plaskett, Interpretation of Fraunhofer-line profiles, Mon. Not. R. Astron. Soc. **115**, 256 (1955).

[18] H. S. W. Massey, Collisions between atoms and molecules at ordinary temperatures, Rep. Prog. Phys. **12**, 248 (1949).

[19] R. K. Janev and Z. M. Radulović, Ion-ion recombination and ion-pair formation processes in alkali-hydrogen diatomic systems, Phys. Rev. A **17**, 889 (1978).

[20] R. E. Olson and M. Kimura, Molecular-state cross-section calculations for $H + Na - H^- + Na^+$, Phys. Rev. A **32**, 3092 (1985).

[21] L. F. Errea, L. Méndez, O. Mó, and A. Riera, Nonadiabatic ionic-covalent transitions. exponential-linear model for the charge exchange and neutralization reactions $Na + H \leftrightarrow Na^+ + H^-$, J. Chem. Phys. **84**, 147 (1986).

[22] A. S. Dickinson, R. Poteau, and F. X. Gadéa, An ab initio study of mutual neutralization in $Na^+ + H^-$ collisions, J. Phys. B: At., Mol. Opt. Phys. **32**, 5451 (1999).

[23] P. S. Barklem, A. K. Belyaev, A. S. Dickinson, and F. X. Gadéa, Inelastic Na+H collision data for non-LTE applications in stellar atmospheres, Astron. Astrophys. **519**, A20 (2010).

[24] K. Lind, M. Asplund, P. S. Barklem, and A. K. Belyaev, Non-LTE calculations for neutral Na in late-type stars using improved atomic data, Astron. Astrophys. **528**, A103 (2011).

[25] A. K. Belyaev, P. S. Barklem, A. S. Dickinson, and F. X. Gadéa, Cross sections for low-energy inelastic H + Na collisions, Phys. Rev. A **81**, 032706 (2010).

[26] A. K. Belyaev and P. S. Barklem, Cross sections for low-energy inelastic H + Li collisions, Phys. Rev. A **68**, 062703 (2003).

[27] E. Herbst, Chemistry in the interstellar medium, Annu. Rev. Phys. Chem. **46**, 27 (1995).

[28] E. Herbst, The chemistry of interstellar space, Chem. Soc. Rev. **30**, 168 (2001).

[29] K. Dolder and B. Peart, Experimental aspects of two-body ion-ion collisions, Rep. Prog. Phys. **48**, 1283 (1985).

[30] N. de Ruette, A. Dochain, T. Launoy, R. F. Nascimento, M. Kaminska, M. H. Stockett, N. Vaeck, H. T. Schmidt, H. Cederquist, and X. Urbain, Mutual neutralization of O^- with O^+ and N^+ at subthermal collision energies, Phys. Rev. Lett. **121**, 083401 (2018).

[31] T. Launoy, J. Loreau, A. Dochain, J. Liévin, N. Vaeck, and X. Urbain, Mutual neutralization in $Li^+ - D^-$ collisions: A combined experimental and theoretical study, Astrophys. J. **883**, 85 (2019).

[32] G. Eklund, J. Grumer, S. Rosén, M. C. Ji, N. Punnakayathil, A. Källberg, A. Simonsson, R. D. Thomas, M. H. Stockett, P.

Reinhed, P. Löfgren, M. Björkhage, M. Blom, P. S. Barklem, H. Cederquist, H. Zettergren, and H. T. Schmidt, Cryogenic merged-ion-beam experiments in desiree: Final-state-resolved mutual neutralization of Li^+ and D^-, Phys. Rev. A **102**, 012823 (2020).

[33] K. R. Lykke, K. K. Murray, and W. C. Lineberger, Threshold photodetachment of H^-, Phys. Rev. A **43**, 6104 (1991).

[34] M. Ciocca, C. E. Burkhardt, J. J. Leventhal, and T. Bergeman, Precision stark spectroscopy of sodium: Improved values for the ionization limit and bound states, Phys. Rev. A **45**, 4720 (1992).

[35] J. F. Baugh, C. E. Burkhardt, J. J. Leventhal, and T. Bergeman, Precision stark spectroscopy of sodium ^2p and ^2d states, Phys. Rev. A **58**, 1585 (1998).

[36] S. Rosén, H. T. Schmidt, P. Reinhed, D. Fischer, R. D. Thomas, H. Cederquist, L. Liljeby, L. Bagge, S. Leontein, and M. Blom, Operating a triple stack microchannel plate-phosphor assembly for single particle counting in the 12–300 K temperature range, Rev. Sci. Instrum. **78**, 113301 (2007).

[37] G. W. Drake, *Springer Handbook of Atomic, Molecular, and Optical Physics*, Springer Handbooks (Springer-Verlag, New York, 2006), 1st ed.

[38] P. S. Barklem, A. M. Amarsi, J. Grumer, G. Eklund, S. Rosén, M. Ji, H. Cederquist, H. Zettergren, and H. T. Schmidt, Mutual neutralization in $Li^+ + H^-/D^-$ and $Na^+ + H^-/D^-$ collisions: Implications of experimental results for non-LTE modeling of stellar spectra, Astrophys. J. **908**, 245 (2021).

[39] R. E. Olson, F. T. Smith, and E. Bauer, Estimation of the coupling matrix elements for one-electron transfer systems, Appl. Opt. **10**, 1848 (1971).

[40] P. S. Barklem, Excitation and charge transfer in low-energy hydrogen-atom collisions with neutral atoms: Theory, comparisons, and application to ca, Phys. Rev. A **93**, 042705 (2016).

[41] P. S. Barklem, Erratum: Excitation and charge transfer in low-energy hydrogen-atom collisions with neutral atoms: Theory, comparisons, and application to Ca [Phys. Rev. A 93, 042705 (2016)], Phys. Rev. A **95**, 069906(E) (2017).

[42] A. Kramida, Yu. Ralchenko, J. Reader, and NIST ASD Team, NIST Atomic Spectra Database (ver. 5.7.1) (National Institute of Standards and Technology, Gaithersburg, MD, 2019), https://physics.nist.gov/PhysRefData/ASD/Html/verhist.shtml, accessed June 1, 2020.

[43] D. A. Dahl, Simion 3D Version 6.0 User's Manual, EG and G Idaho, Inc., Idaho Falls, ID, 1995, https://www.osti.gov/biblio/130674.

Correction: Affiliation indicators for the fourth through tenth authors were set incorrectly during production and have been fixed.